Archaeological Prospection
Archaeol. Prospect. **22**, 45–62 (2015)
Published online 31 October 2014 in Wiley Online Library
(wileyonlinelibrary.com) DOI: 10.1002/arp.1497

A Template-matching Approach Combining Morphometric Variables for Automated Mapping of Charcoal Kiln Sites

ANNA SCHNEIDER[1]*, MELANIE TAKLA[2], ALEXANDER NICOLAY[1], ALEXANDRA RAAB[1] AND THOMAS RAAB[1]

[1] *BTU Cottbus-Senftenberg, Chair of Geopedology and Landscape Development, Konrad-Wachsmann-Allee 6, D-03046 Cottbus, Germany*
[2] *BTU Cottbus-Senftenberg, Research Center Landscape Development and Mining Landscapes (FZLB), Konrad-Wachsmann-Allee 6, D-03046 Cottbus, Germany*

ABSTRACT Analysing the spatial distribution of anthropogenic relief structures can contribute to the understanding of past land-use systems. With automated mapping routines, small relief forms can be detected efficiently from high-resolution digital terrain models (DTMs). In this study, we describe an approach for the automated mapping of charcoal kiln sites from an airborne laser-scanning DTM. The study site is located north of Cottbus, Germany, where an exceptionally large historic charcoal production field has been documented in previous archaeological surveys. The goal of this study was to implement, evaluate and improve an automated GIS-based routine for mapping these features based on the template-matching principle. In addition to the DTM, different morphometric variables were evaluated for their suitability to detect kiln sites. The mapping results were validated against a comprehensive database of kiln sites recorded from archaeological excavations and via manual digitization. The effects of irregular kiln-site geometry and DTM noise were evaluated using synthetic DTMs. The results of the synthetic DTM mapping show that the template-matching results differed depending on the morphometric variable used for the mapping process. In accordance with this observation, a validation of the mapping procedure for the field site suggests that feature mapping can be improved. In particular, the number of false detections can be reduced using a combination of morphometric variables. For the validation area, the kiln sites with diameters of at least 10 m were mapped using the automated routine, with detection rates that were close to those of manual digitization. Therefore, the described method can considerably facilitate the mapping and distribution analysis of kiln sites or similar small relief forms that are prominent in a specific landscape. Copyright © 2014 John Wiley & Sons, Ltd.

Key words: Digital elevation model; template matching; charcoal kilns; geoarchaeology; airborne laser scanning; small landforms

Introduction

Human settlement and land use result in small-scale terrain modifications. Anthropogenic relief features occur in prehistoric and historic settlement areas or burial sites, for example, settlement mounds (Menze *et al*., 2006) or pitfall traps (Trier and Pilø, 2012), or they result from land use, for example, characteristic shapes resulting from charcoal production. Historic charcoal production sites are characterized by pits that were dug for kilns that were constructed at least partly in the ground or by the remains of upright charcoal hearths and kilns that were installed above the ground (Groenewoudt, 2005). Charcoal pits can be circular or rectangular and are typically only a few metres across. Such pit kilns have been described for relatively old charcoal production areas in Norway (Bollandsås *et al*., 2012; Risbøl *et al*., 2013), the Netherlands (Groenewoudt, 2005) and northeastern Germany (Lipsdorf, 2001). From the sixteenth to seventeenth centuries upright charcoal hearths replaced pit kilns in most areas (Lipsdorf, 2001; Bond, 2007). Such upright kilns were constructed on planar surfaces, resulting in characteristic platforms or

*Correspondence to: A. Schneider, BTU Cottbus-Senftenberg, Chair of Geopedology and Landscape Development, Konrad-Wachsmann-Allee 6, D-03046. Cottbus, Germany. E-mail: schneida@tu-cottbus.de

Received 12 June 2014
Accepted 21 September 2014

terraces on slopes in mountainous areas, as described by Nelle (2003) and Ludemann (2003) in the Bavarian and Black Forests, or in small mounds in flat areas, as described by Bond (2007) and Deforce *et al*. (2013) for sites in England and Belgium. The remains of upright kilns mainly have circular ground plans, although oval ground plans were observed and associated with repeatedly used sites by Bond (2007). Mapping these sites is important for analysing past land-use systems and can improve the understanding of past land use, tree-harvesting patterns and the associated effects on landscapes and ecosystems.

High-resolution elevation data from airborne laser-scanning (ALS) can capture relatively small relief forms, even in forested areas where features are typically preserved. Therefore, ALS-based digital terrain models (DTMs) are frequently used for the detection of anthropogenic relief structures (Hesse, 2010; Deforce *et al*., 2013; Risbøl *et al*., 2013). Most approaches for visualizing anthropogenic and other small relief structures in DTMs are based on illumination simulation techniques, such as the use of hillshade or shaded-relief maps (Bennett *et al*., 2012: Stular *et al*., 2012; Schindling and Gibbes, 2014). In addition, enhanced visualization methods based on illumination simulations, such as hillshade principle component analysis (Devereux *et al*., 2008), a combination of hillshade maps or the sky-view factor with slope maps (Kennelly, 2008; Stular *et al*., 2012), have been used for manual mapping. The local-relief model developed by Hesse (2010) enhances the visibility of morphological features by representing local elevation differences. Several other variables are commonly used in geomorphology to describe relief structures; however, these variables are less frequently applied in archaeological studies. Maps generated with such visualization techniques are frequently used for mapping relief features via manual digitization. However, to map structures that are numerous in a landscape, manual digitization can be excessively time-consuming, and therefore (semi-) automated approaches are required.

Many studies have addressed automated DTM classification or feature extraction for geomorphological mapping. Generally, the suitability of the methods for automated feature extraction is dependent on the geometry of the object to be detected. Segmentation and object-based image analysis can be used to map features with clearly different morphometric characteristics relative to the surrounding terrain. Segmentation methods have been used for the semi-automated extraction of different geomorphical features from high-resolution ALS DTMs, for example, landslide bodies (Van Den Eeckhaut *et al*., 2012), gullies (Shruthi *et al*., 2011) or drumlins (Eisank *et al*., 2014); these methods have also been used in landform classification for archaeological mapping (Verhagen and Drăguţ, 2012). Differentiating features with similar morphometric characteristics can also be addressed via statistics-based processing and DTM classification; these techniques were used by Tarolli *et al*. (2012) to extract landslide features and by Sofia *et al*. (2014) to extract linear anthropogenic features. Using the geomorphological phonotype (geomorphon) approach, Jasiewicz and Stepinski (2013) described a pattern-recognition method for the detection of geomorphological features. Numerous studies address the automated extraction of lunar or Martian craters from remote-sensing images or DTMs (Sawabe *et al*., 2006; Bandeira *et al*., 2012; Salamunićcar *et al*., 2014). These methods often require large databases of training images, or they are designed to detect exact circular shapes and strong illumination contrasts. De Laet *et al*. (2007) evaluated automated detection by edge-enhancement filtering and pixel- and object-based classification for the extraction of archaeological features from satellite imagery; they noted that these methods have been applied only sparingly in archaeology. Similarly, the numerous methods for automated mapping from DTMs have not been widely applied for detecting specific anthropogenic relief features.

For mapping specific locally concentrated features with a characteristic geometry, template-matching approaches can be applied. In these approaches, a prototype pattern or template with the characteristic structure of the features of interest is constructed and then a matrix of correlations between these templates with the image or elevation-model pixels is calculated for a moving window. The highest correlation values are then extracted from the correlation matrix and transferred to the feature maps. Using templates with different sizes, the size of the detected feature can be recorded. The sum of the squared differences between template and image pixels can be used to compute the correlation when the similarity between the template and the feature to be detected is very high. In most studies, however, normalized cross-correlation is used to obtain the correlation matrix (Pirotti, 2010; Trier and Pilø, 2012). In template matching, the cross-correlation is normalized by subtracting the mean and dividing by the standard deviation of the search-window area in the image when using photographs to compensate for variations in image brightness and contrast, respectively. When working with elevation models, subtracting the mean compensates for larger-scale elevation differences around the features of interest, for example, for a sloping terrain around the features, such that template matching can be conducted without applying trend removal to

DOI: 10.1002/arp

the DTM. Normalization via dividing by the standard deviation compensates for differences in the range of elevations within the template window, such that features of different absolute heights can be recorded.

Template matching is particularly well suited for mapping circular structures because correlation matrices can be computed without rotating the template. Mapping circular features via template matching has been described for high-resolution satellite images by Trier *et al*. (2009) and by Trier and Pilø (2012) for mapping pit structures from ALS data. A template-matching approach was also used by Pirotti (2010) for mapping tree positions from canopy-height models, by Nyström *et al*. (2014) for the detection of wind-thrown trees using a differential elevation model, and by Pollock (1998) to detect individual trees in aerial images.

The application of template matching for feature detection in DTMs typically results in many false positive detections, as was shown in several of the aforementioned studies and was similarly noted by Menze *et al*. (2006). For relief features that occur at a high frequency, numerous false positive detections imply that the mapping results must be visually evaluated and corrected with substantial effort.

In this study, we implemented and evaluated a template-matching approach to map morphological structures remaining at charcoal kiln sites. The study area (Figure 1) is an exceptionally large charcoal-production field north of Cottbus, Germany, in which kiln-site mapping has been performed previously in archaeological excavations and by manual digitization from hillshade maps. To extend the findings for this charcoal-production field to larger areas, we attempted to implement an automated routine that allows for efficient mapping of the kiln sites and their diameters within a GIS environment in order to map the kiln sites for larger areas. The initial efforts to apply a template-matching detection to the area indicated that false positive detections were more numerous than true detections. Manually removing these false positives would be very time-consuming because of the high density of the features. Therefore, the development of a routine for improved mapping of the relief features by template matching with fewer false positive detections would be desirable. A thorough visual inspection of the elevation models showed that most kiln sites were most visible in hillshade maps; however, particular sites that could not be identified clearly from these maps could be better detected from maps of other morphometric variables, for example, the slope or the topographic position index. Therefore, we attempted to use different morphometric variables for automated mapping.

The primary goals of this study were to: (i) implement an automated routine for feature detection using template matching in GIS; (ii) evaluate different morphometric variables for their suitability for detecting kiln sites using template matching; and (iii) reduce the ratio of false positive to true positive detections in the template-matching routine.

For the study site, a nearly complete kiln-site map already exists, based on excavations over an area of approximately 17 km^2. Along with the kiln-site dataset that was previously digitized using a detailed visual analysis of a hillshade map computed with four different illumination settings (Raab *et al*., 2014), an exceptionally good database is available to develop and validate automated mapping approaches.

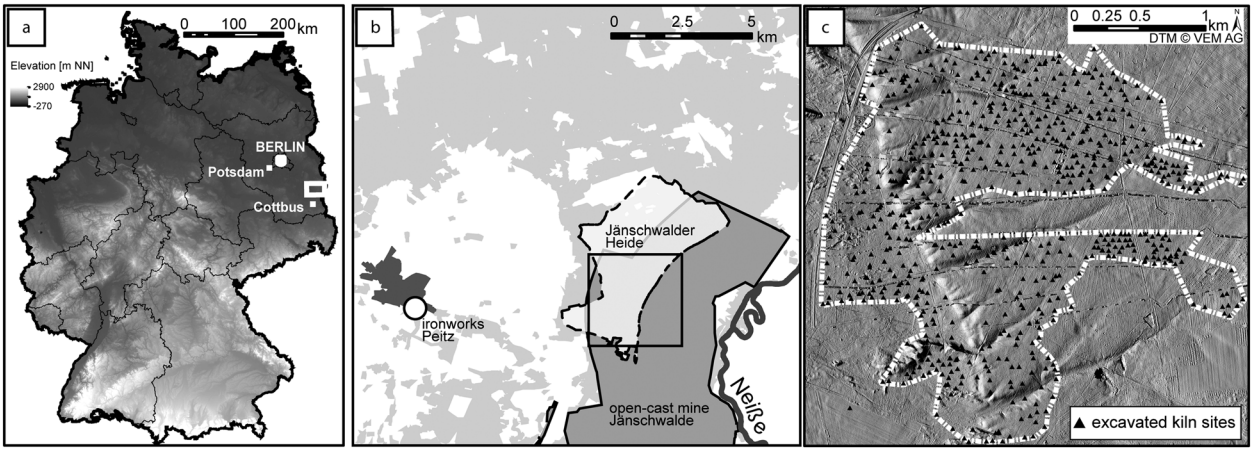

Figure 1. (a) Location of the study site north of Cottbus, Germany. (b) Location of the study site in relation to Jänschwalde opencast mine. (c) Delineation of the validation area around the excavated kiln sites.

DOI: 10.1002/arp

Material and methods

Study site and database

The study area is located within the North German Lowland, approximately 15 km northeast of Cottbus and approximately 150 km southeast of Berlin (Figure 1a and b). The geomorphology is characterized by relatively flat terrain that was formed by Quaternary glacial and periglacial processes. The maximum extension of the delimited validation area is approximately 3 km in the W–E and S–N directions (Figure 1c). The elevation increases from approximately 63 m a.s.l. in the west to approximately 87 m a.s.l. in the east. Single drainage lines are incised into the terrain from the slightly higher terrain of the Taubendorfer Sandur to the lower terrain of the Spree River lowlands in the westernmost part of the area. Smaller-scale topography within the validation area is characterized by anthropogenic structures from prehistoric and historic land use (Nicolay *et al*., 2014) and by recent structures from forestry and preparatory earthworks for mining, for example, structures along forest planting rows, tracks, or spoil heaps.

The charcoal-kiln field examined is situated adjacent to the Jänschwalde open-cast lignite mine, which is northeast of the Peitz village. Charcoal was used in an ironworks that operated from the sixteenth to the nineteenth centuries in Peitz (Rösler, 2008). Charcoal production in the area has been described by previous archaeological research (Rösler *et al*., 2012) adjacent to the active mine. In these archaeological excavations, a considerably high density of charcoal-kiln sites has been described in the Jänschwalder Heide royal forest area. An examination of the ALS DTM suggests that the surrounding areas contain a similarly high density of kiln sites. Previously, approximately 5500 kilns were detected in an area of 32 km^2 according to the ALS DTM, and approximately 800 kilns have been verified by archaeological excavations in an area of approximately 17 km^2 adjacent to the mine (Raab *et al*., 2014). Similarly high densities of kiln remains have not been described for other areas in the northern European lowlands.

The kiln-site geometry in the study area (Figure 2a) is typically characterized by the remnants of a ditch surrounding the charcoal kiln and by a wood stack in the centre, which shows that charcoal was produced in circular, upright kilns. After clearing the kiln sites, the ditches were mostly filled with charcoal; therefore, they are only slightly lower than the surrounding terrain. The central mounds are typically flattened and have a plateau-like shape with elevation differences of a few decimetres compared with the surrounding terrain. The kiln relics' inner diameters documented from excavations in the Jänschwalder Heide area range from 3 m to 29 m, with an average diameter of 12.4 m (Raab *et al*., 2014). The kiln geometry has been preserved to various degrees, as shown in the kiln ground plans documented in archaeological excavations (Rösler *et al*., 2012) in which the complete circular structure of the charcoal-filled ditch has been observed for certain sites, but only fractions of the circular structures have been found at other sites.

To map the kiln sites we used DTMs based on ALS data with a 1 m horizontal resolution provided by

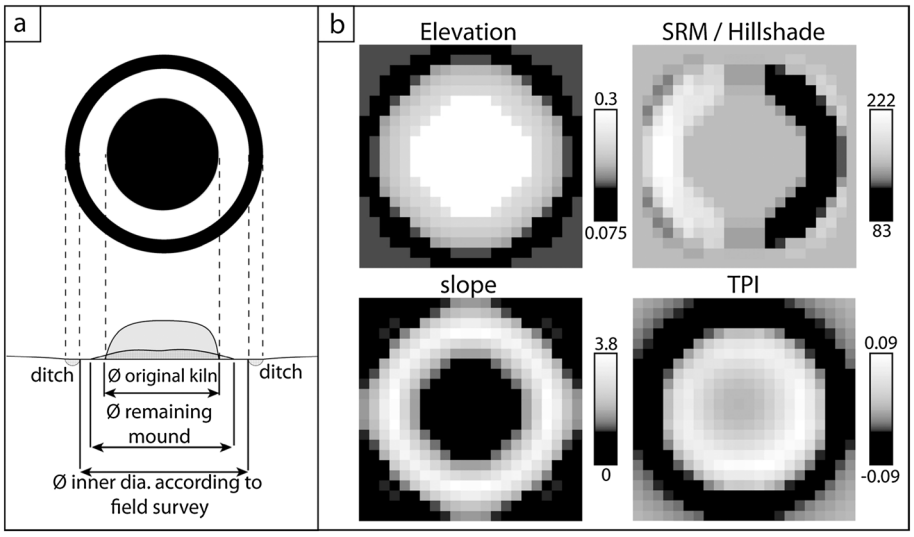

Figure 2. (a) The ground plan and cross-section geometry of a charcoal kiln site. (b) The elevation, slope, topographic position index and hillshade values for a kiln template with an inner diameter of 18 m.

DOI: 10.1002/arp

Vattenfall Europe Mining AG. The ALS data were recorded in 2003 and 2008 from an altitude of 850 m and 600 m, respectively, with a target ground-point density of four points per square metre. For validation, we used a database of the centre coordinates and diameters for 864 kilns that were documented in archaeological excavations by the Brandenburg archaeological survey (Brandenburgisches Landesamt für Denkmalpflege und Archäologisches Landesmuseum, BLDAM) between 2005 and 2013 in the mine area. Furthermore, the results were validated against kiln sites that were manually digitized using a visual hillshade map analysis based on the same DTM (Raab *et al*., 2014).

Template and synthetic DTM construction

The DTM processing and template construction were performed using ArcGIS 10 (ESRI, Redlands, California) and SAGA (SAGA User Group Association, Göttingen). The kiln-site templates were defined for diameters from 8 m to 28 m in 1 m increments. We used specifically constructed templates for each diameter because we assumed that the geometry of the kiln remains cannot be scaled proportionally to the diameter, for example, the width of the surrounding ditch is not smaller for smaller kiln sites. The idealized geometry of a kiln site was derived from analyses of the geometry of numerous kiln sites depicted in elevation models and from GPS measurements and observations obtained during previous field work at kiln sites. For those kiln sites within the study area that were previously mapped manually from hillshade maps (Raab *et al*., 2014), the mean range of the DTM values was 0.3 m (±0.2 m), and slightly lower elevation ranges were observed for smaller kiln sites. The kiln-site templates were therefore constructed so that the ditch surrounding the kiln was 0.05 m lower than the surrounding surface and the elevation of the mound increased towards the kiln plateau in two increments up to 0.2 m (for diameters up to 13 m) or in three increments up to 0.25 m (for diameters of at least 14 m) above the surrounding surface (Figure 2b).

In addition to the ALS DTM, we used synthetic DTMs to evaluate the effects of the deviations from ideal kiln-site geometry and general inaccuracies (noise) in the elevation data on the correlations computed using template matching and the mapping results. A DTM representing kiln remains with a non-ideal geometry (Figure 3a) was constructed by superimposing several template models with diameters of 12, 18 and 24 m to a surface with an inclination of 0.05% from west to east, which is similar to the slope of the ALS DTM (Figure 3a, left side) and to a horizontal surface (Figure 3a, right side). Different irregularities that were frequently observed in the kiln sites in the ALS DTM were subsequently modelled on the kiln templates (e.g. a kiln with incomplete preservation of the circular shape, depressions resulting from a funnel in the centre of the kiln mound, irregular kiln plateaus, and partially or completely filled kiln ditches) and on the surface around the templates (e.g. pits or spoil heaps). Furthermore, characteristic objects that presumably provoke false positive kiln site detections (e.g. large spoil heaps or crossing linear structures) were included; Gaussian noise with a standard deviation of 0.05 m was added to the model to simulate the ALS DTM inaccuracies. To evaluate the effects of DTM noise, another synthetic DTM representing the kiln templates for diameters from 8 to 28 m was

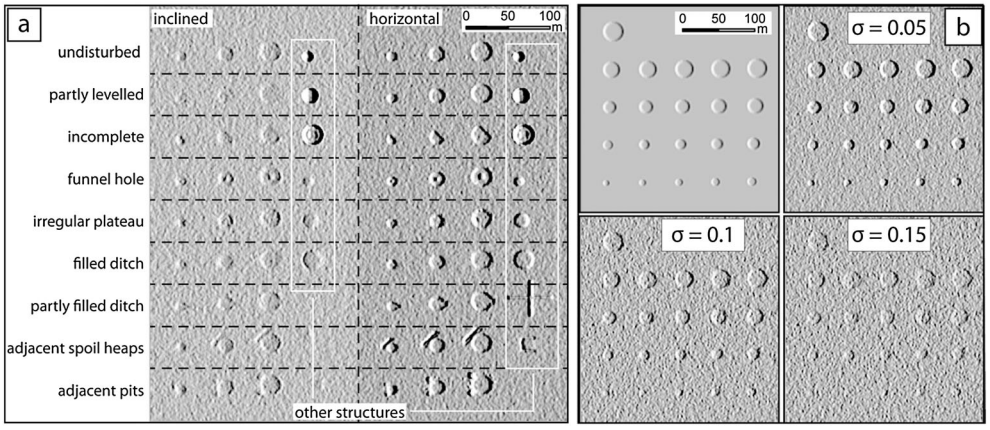

Figure 3. Hillshade maps for (a) a synthetic DTM representing the disturbed kiln sites with diameters of 12, 18 and 24 m and other surface structures on a sloping (left side) and horizontal (right side) surface, and (b) a synthetic DTM representing kiln sites with diameters of 8–28 m without noise and with low, moderate and high Gaussian noise.

DOI: 10.1002/arp

constructed; Gaussian noise was added with standard deviations of 0.05, 0.1 and 0.15 m (Figure 3b).

As the visual analysis exhibited relatively substantial irregularities in the ALS DTM, a low-pass filter was applied to reduce noise and enhance the feature visibility. The same filter was correspondingly applied to the synthetic DTM and the kiln-site templates. The following morphometric variables were then computed for the DTM and the templates: (i) hillshade maps with an illumination azimuth of 270°, an elevation of 40 °, and a fivefold superelevation to increase the contrast; (ii) slope; and (iii) the topographic position index (TPI) using the land facet corridor tool (Jenness *et al*., 2013) for a circular neighbourhood with a radius of 10 m.

Workflow for automated detection

The automated detection routine was implemented in ArcGIS using functions from ArcPy and the image processing module from the OpenCV (Open Source Computer Vision, Version 2.4, OpenCV Development Team, 2014) library. The DTM was divided into tiles of 2048×2048 pixels (e.g. approximately 4 km^2 for the 1 m DTM with an overlap of 20 m) to be used as the image in the template-matching function. As an initial step (Figure 4), the DTM and template rasters were transformed into NumPy arrays. The OpenCV template-matching function was then used to calculate the normalized cross-correlation C between the kiln templates T and the terrain model M for each pixel (x, y) according to the following equation:

$$C(x,y) = \frac{\sum_{x',y'}[T'(x'y') - M'(x+x', y+y')]}{\sqrt{\sum_{x',y'}\left[T'(x',y')^2 \cdot \sum_{x',y'} M'(x+x', y+y')\right]^2}}$$

where $T'(x',y')$ and $M'(x+x',y+y')$ are the template and terrain-model pixel values subtracted by the mean values for the template and terrain model within the template kernel, respectively; these values are computed according to the following equations:

$$T'(x',y') = T(x',y') - 1/(w \cdot h) \cdot \sum_{x'',y''} T(x'',y'')$$

and

$$M'(x+x', y+y') = M(x+x', y+y') - 1/w \cdot h) \cdot \sum_{x'',y''} M(x+x'', y+y''),$$

where w and h are the width and height of the template kernel (in number of pixels), respectively. A fully normalized cross-correlation was chosen to obtain the correlation matrix to compensate for: (i) the increase in elevations from the western to the eastern parts of the study area; and (ii) the differences in kiln-site heights, which were observed in preliminary analyses of the site geometry and are assumed to result from a progressive subsidence or levelling of the kiln remains. The correlation matrices are then filtered so that only the following are maintained: (i) the maximum correlation within a circular window with a diameter of twice the template diameter; and (ii) values that exceed a user-defined correlation threshold. The remaining values are transformed to a point dataset, and the correlation and kiln diameter are added to each point as an attribute. After

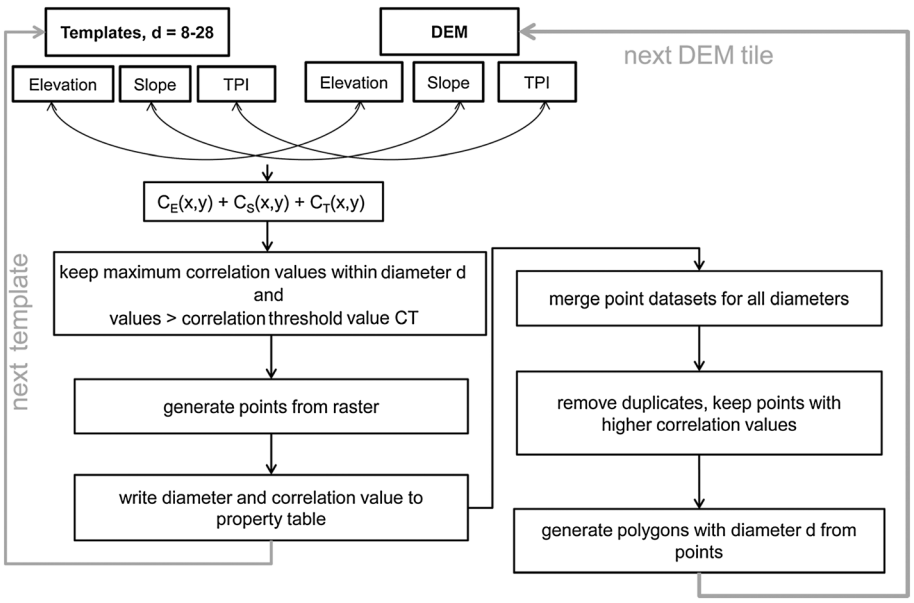

Figure 4. Workflow for the automated kiln-site detection routine, which is exemplified here for a combination of three morphometric variables.

DOI: 10.1002/arp

repeating this workflow for each kiln diameter, the point datasets are merged, and duplicate detections within a defined circular window are deleted so that the detections with the highest correlations remain. For the example of the Jänschwalde area, detections with a distance of less than 16 m apart were considered to be duplicate detections based on the observation that only large kiln sites occurred immediately adjacent to each other. As a final step, polygons are created from the detected kiln centre points by applying a buffer function using the kiln radius as the buffer distance.

We performed this detection routine repeatedly using the elevation values, the slope maps, the TPI and the hillshade map as the image and template datasets. Furthermore, the detection was performed for all possible combinations of the variables by adding the correlation matrices computed for each variable and adjusting the correlation threshold value to the number of variables. The basic statistics of the elevation values and the morphometric variables were determined within the mapped polygons from the DTM and its derivatives to characterize the mapping results.

Validation and evaluation of the mapping results

The area used to evaluate the map results was defined based on the location of the excavated kiln ground plans that were used as the reference dataset. Although previous excavations were conducted systematically over the mine area, they did not cover a completely continuous area. Therefore, a polygon was drawn around the largest spatially contiguous group of excavated kiln sites. A total of 741 of the documented kiln-site data points were located within this area; 632 of these sites had a documented inner diameter of at least 7.5 m and could be used to validate the mapped locations and diameters. For 48 additional kilns, no inner diameter was recorded in the excavations; however, the diameters could be determined and added to the dataset according to the results of the manual digitization from the hillshade map so that these sites could also be used to validate the location of the detections. As an initial visual inspection suggested that considerably more small relics were mapped than large kiln relicts, we considered three diameter classes in the evaluation, that is, all of the resulting detections with diameters of at least 8 m and only those detections with diameters of at least 10 m or at least 12 m; subsets of the validation data with inner diameters of at least 7.5 m, 9.5 m or 11.5 m, respectively, were assigned to these detection subsets. To evaluate the accuracy of the diameters mapped, differences in the inner diameters that were documented according to the excavations were determined for the detections coinciding with the excavated kiln sites. Moreover, basic quality criteria (the root mean square error, RMSE, and the mean error, ME) were calculated.

We defined the detections that coincided with the excavated kiln sites as true positive detections. The identifications that did not coincide with the kiln-site locations documented from the excavations were considered to be false positive detections (commission errors). Despite the comprehensive dataset available for validation in the mine area, certain limitations must be considered. First, it cannot be excluded that certain kiln sites were not documented in the archaeological excavations, which can cause an overestimation of false detections. Furthermore, false negative detections or omission errors can result from DTM mapping because complete kiln-site levelling due to land use after charcoal production may have occurred; therefore, all kiln sites found in the archaeological excavations may not actually be present as morphological structures and cannot necessarily be found in the elevation models. The kiln-site morphology may have been destroyed or obstructed by earthworks in the mine area before the ALS data recording. As the manual kiln-site mapping from the DTM was performed using a thorough approach by repeated mapping of the kiln sites from the hillshade map generated with different illumination settings (Raab *et al.*, 2014), we presume that the detections achieved by manual mapping represent nearly all detectable sites.

RESULTS

Detection results for the Jänschwalde validation area

The mapping results for the ALS terrain model exhibited clear differences between the results of mapping with different variables and variable combinations. Mapping and evaluation of the results were conducted for all possible combinations of the morphometric variables (elevation, slope, hillshade, and TPI). A preliminary evaluation showed that the best results were achieved with the combination of *elevation–slope* when using two variables, with the combinations of *elevation–slope–TPI* or *hillshade–slope–TPI* when using three variables, or with the combination of all four variables. Therefore, we present and discuss the evaluation results for these combinations. The false positives rapidly decreased for increasing correlation thresholds up to approximately 0.6 and decreased more gradually

DOI: 10.1002/arp

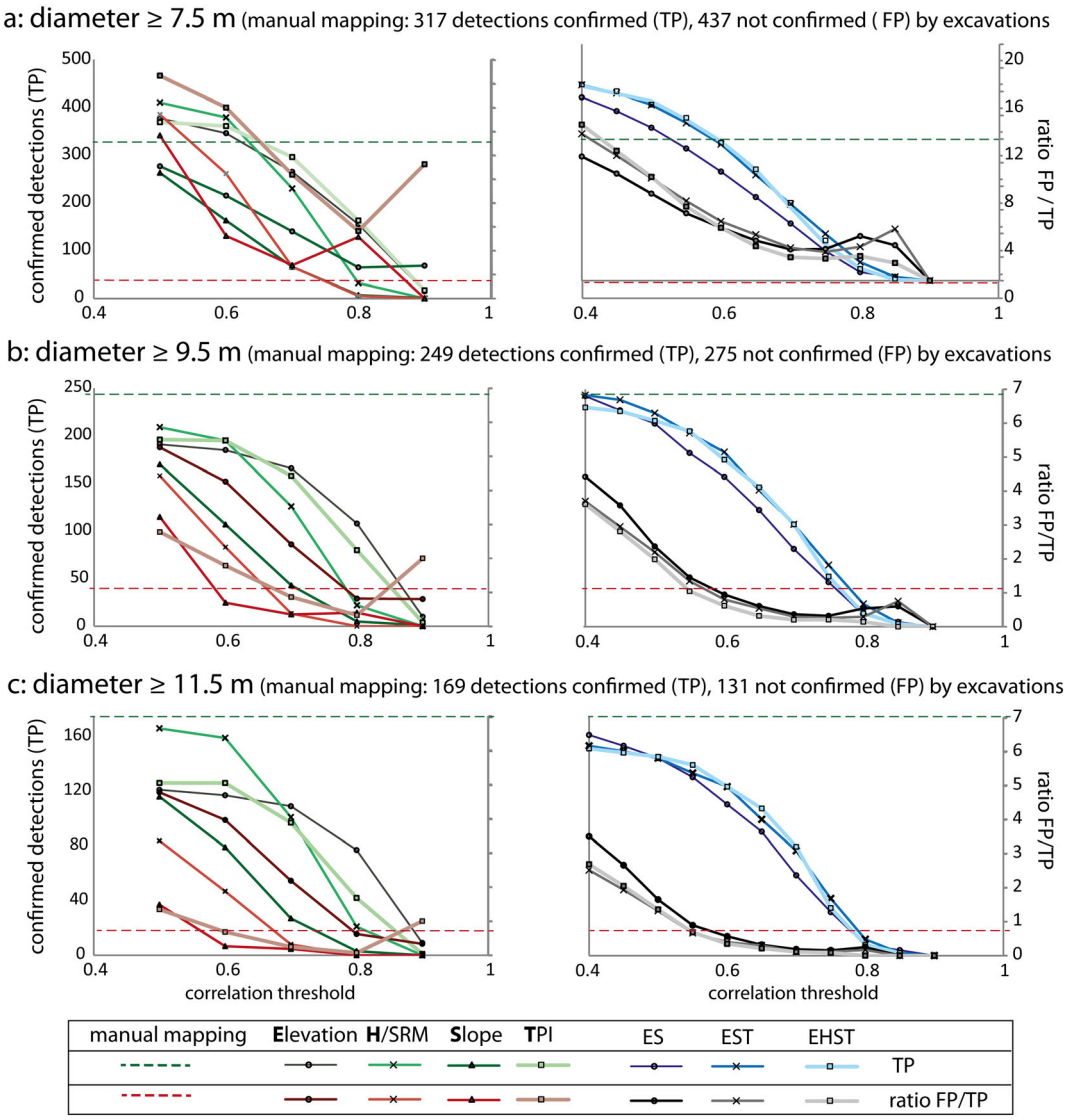

Figure 5. Number of true positive detections (left axes) and the ratio of false positive to true positive detections (right axes) as a function of the correlation threshold value for the different variable combinations for all kiln sites with diameters (a) ≥7.5 m, (b) ≥9.5 m and (c) ≥11.5 m compared with the results for manual mapping from the Hillshade map (dashed horizontal lines). The results for a detection threshold of 0.4 were not evaluated for the single variables because of numerous false detections.

for the higher range of correlation thresholds (Figure 5). In contrast, the number of true detections decreased more slowly for the lower range of correlation thresholds and more rapidly for the higher range. This result was most pronounced for kiln-site diameters ≥11.5 m (Figure 5c). The number of true and false positives varied considerably between the single variables (Figure 5, left side). Most correct detections were attained using the hillshade for the lower correlation threshold range and using the TPI and elevation for the higher threshold range; the detections were fewest when using the slope. However, mapping based on the slope produced fewer false than true detections even for a relatively low correlation threshold, whereas other variables primarily resulted in more false than true detections. For the relatively well-performing variable combinations shown in Figure 5, the number of true detections was similar; however, more false positives were produced by mapping with the *elevation–slope* combinationcompared with combinations of three or four variables (Figure 5, right side). Generally, most true detections were achieved using the *elevation–slope–TPI* combination. The fewest false positives resulted with the *elevation–slope* combination for diameters ≥7.5 and with the *hillshade–slope–TPI* combination for diameters ≥9.5 m. Automated

DOI: 10.1002/arp

Table 1. Detection results for template matching using the elevation values and the combination of elevation, slope and TPI for kiln-site diameters (Ø) ≥9.5 m and ≥11.5 m. The results for a detection threshold of 0.4 were not evaluated for the elevation because of the numerous false detections.

Variable	Detection threshold	Ø 9.5–28 m				Ø 11.5–28 m			
		True positive detections		False positive detections		True positive detections		False positive detections	
		n	Percentage of excavatedkilns (*n* =554)	*n*	Percentage of total detections	*n*	Percentage of excavated kilns (*n* =423)	*n*	Percentage of total detections
Hillshade (manual mapping)		249	45	275	53	169	40	131	44
Elevation	0.5	191	34	1005	84	121	29	577	83
	0.6	185	33	787	81	117	28	463	80
	0.7	166	30	40	71	109	26	238	69
	0.8	108	20	88	45	77	18	48	38
	0.9	10	2	8	44	9	2	3	25
Elevation–slope– TPI	0.4	244	44	904	79	154	36	387	72
	0.5	225	41	495	69	145	34	191	57
	0.6	184	33	148	45	124	29	49	28
	0.7	108	20	32	23	77	18	9	11
	0.8	24	04	7	23	12	3	2	14
	0.9	0	0	1	100	0	0	0	0

mapping generally produced more false detections than manual mapping. A comparison of the automated detection results for template matching using the elevation values and the *elevation–slope–TPI* combination (Table 1) demonstrates that at a correlation threshold of 0.6, the number of false positives is reduced by approximately 80% and approximately 90% for diameters ≥9.5 m and ≥11.5 m, respectively, using the variable combination. Moreover, the number of true detections for the variable combination is nearly as high and even higher when considering diameters ≥9.5 m and ≥11.5 m, respectively.

The quality criteria for the deviations between the mapped diameters and those documented from the excavations (Table 2) suggest that the kiln-site diameters are generally underestimated using the template-matching approach regardless of the variables used. The ME and the RMSE were highest for template matching when only elevation was used. For single variables, the greatest accuracy was achieved with the slope or the TPI depending on the evaluated diameter range. For the variable combinations, the smallest deviations resulted for the *elevation–hillshade–slope–TPI* and *hillshade–slope–TPI* combinations; however, the variable combinations did not improve the accuracy compared with the single variables. Although the diameters also appeared to be underestimated via manual mapping, the underestimation was primarily higher when the automated detection algorithm was applied. A slightly lower RMSE compared with the manual mapping approach was achieved only for

Table 2. Quality criteria for the mapped diameters (Ø) compared with the inner diameters recorded for the excavated kilns. There were 632, 507 and 384 excavated kilns with documented inner diameters ≥7.5 m, ≥9.5 m and ≥11.5 m, respectively. The detections for a correlation threshold of 0.5 were evaluated for all variables and variable combinations.

Variable	Ø 7.5–28 m			Ø 9.5–28 m			Ø 11.5–28 m		
	n	RMSE	ME	*n*	RMSE	ME	*n*	RMSE	ME
Elevation	343	4.18	−2.91	173	3.82	−2.47	103	3.55	−1.85
Hillshade	373	3.00	−1.57	189	2.54	−0.91	146	2.37	−0.58
Slope	243	2.71	−1.14	163	2.72	−0.88	108	2.62	−0.45
TPI	330	3.18	−1.97	171	2.36	−1.31	106	1.9	−0.9
E–S	293	3.29	−1.55	196	3.33	−1.29	129	3.19	−0.63
E–S–T	338	3.1	−1.75	204	2.93	−1.48	126	2.42	−0.79
H–S–T	342	2.89	−1.61	195	2.62	−1.29	128	2.22	−0.69
E–H–S–T	338	3.03	−1.73	192	2.77	−1.32	126	2.31	−0.6
Hillshade (manual mapping)	283[a]	2.77	−0.9	237	2.82	−0.76	158	2.66	−0.31

RMSE, root mean square error; ME, mean error; E, elevation; H, hillshade; S, slope; T, TPI.
[a]The lower number of detections for manual mapping partially resulted from not including kiln sites mapped with diameters <7.5 m in the evaluation.

DOI: 10.1002/arp

Table 3. Basic statistics for the elevation and slope values within the mapped polygons and the correlation values of the true and false positive detections (mapped with the combination of elevation, slope and TPI and a correlation threshold of 0.4).

Statistic	Ø 7.5–28 m (mean ± standard deviation)		Ø 9.5–28 m (mean ± standard deviation)	
	True positive detections	False positive detections	True positive detections	False positive detections
Range of elevations	0.26 ± 0.22	0.38 ± 0.48	0.29 ± 0.22	0.47 ± 0.63
Minimum of slope values	0.26 ± 0.33	0.61 ± 1.03	0.17 ± 0.18	0.32 ± 0.7
Mean of slope values	2.25 ± 1.7	3.79 ± 4.82	2.08 ± 1	3.54 ± 5.03
Summed correlation	1.97 ± 0.33	1.65 ± 0.31	2.01 ± 0.31	1.56 ± 0.25

Ø, diameter.

certain variables and variable combinations and for the larger kiln-site classes.

The elevation ranges, which describe the heights of the mapped features, and the mean slopes within the mapped polygons were found to differ between true and false detections (Table 3). For mapping using the *elevation–slope–TPI* combination with a relatively low correlation threshold of 0.4, the range of elevation values within the true positive polygons was lower and exhibited less variation than that for the false positives. This result indicates that many false detections occurred at round spoil heaps, which are primarily higher than kiln remains. The minimum and mean slope values in the true detection polygons were considerably lower than those for the false detections, which reflect a characteristic kiln-site plateau. It was also found that the mean correlation between the templates and the DTM was clearly higher for the true compared with the false detections. These differences were observed when considering all of the mapped diameters and were more pronounced when considering only diameters of at least 9.5 m.

Mapping results for synthetic DTMs

The results of template matching for the synthetic DTM with the disturbed kiln features enable a comparison of the general detection quality for different variables (Tables 4 and 5) and an evaluation of the effects of specific geometry disturbances on the mapping results (Table 6).

The maximum correlations between the templates and the DTM for the synthetic DTM depicting disturbed kiln sites without any additional noise are provided for diameter (Ø) =18 m in Table 4. The deviations in the feature geometry affected the correlations to different extents depending on the variable used for mapping. On flat terrain, the correlations were generally highest using the elevation values. However, on a sloping terrain, the correlations were higher for the other variables, primarily for the TPI. This result suggests a higher sensitivity of elevation to the variations in the overall topography of the area surrounding the features when using the template-matching method.

The mapping results for the synthetic DTM depicting the disturbed kiln sites with low DTM noise (shown in Table 5 for the single variables and the best-performing variable combinations) further confirm that using different variables for template matching can generate largely different maps. Several kiln sites could not be mapped using the slope, hillshade or TPI for this DTM due to the additional geometry disturbance induced by the DTM noise, whereas all the features were detected when using elevation (Table 5). Missing detections still occurred for certain combinations of two variables (the combinations of *slope–TPI*, *slope–hillshade* and *hillshade–TPI*; data not shown), whereas all the

Table 4. Correlations between the templates and the kiln sites (Ø =18 m) in a synthetic DEM for different types of deviations from the template geometry; the results were computed for different diameters.

Landscape feature	Sloping terrain				Flat terrain			
	Elevation	Slope	Hillshade	TPI	Elevation	Slope	Hillshade	TPI
Undisturbed	0.89	0.88	0.89	0.91	1	1	0.99	1
Partially levelled on sloping terrain	0.62	0.64	0.72	0.8	1	1	0.99	1
Incomplete kiln site	0.74	0.54	0.62	0.77	0.82	0.51	0.57	0.74
Funnel hole	0.82	0.67	0.78	0.81	0.93	0.74	0.86	0.87
Irregular plateau	0.71	0.37	0.61	0.66	0.86	0.65	0.69	0.8
Levelled ditch	0.83	0.85	0.89	0.92	0.99	0.95	0.97	0.98
Partly filled ditch	0.82	0.81	0.79	0.87	0.91	0.83	0.77	0.86
Adjacent spoil heaps	0.87	0.8	0.84	0.86	0.89	0.8	0.87	0.87
Adjacent pits	0.78	0.47	0.71	0.74	0.87	0.58	0.77	0.8

DOI: 10.1002/arp

Table 5. Detection quality for disturbed features with Ø =12 m, 18 m and 24 m in a synthetic DEM; the table compares the results for single variables and variable combinations.

Variable	Number of features not detectable	Minimum correlation threshold for the detection of all other features	Number of false positive detections at the minimum correlation threshold	Number of features with correctly mapped diameters	Sum of deviations between mapped and feature diameters
Elevation	0	0.59	45	23	21
Hillshade	7	0.62	23	23	55
Slope	6	0.46	72	28	32
TPI	4	0.58	99	27	38
E–S	0	0.54	10	28	38
E–S–T	0	0.56	14	30	34
H–S–T	0	0.53	18	30	38
E–H–S–T	0	0.55	14	29	35

E, elevation; H, hillshade; S, slope; T, TPI.

features were detected using combinations of three or four variables. Clear differences were observed in the number of false positive detections that resulted when the selected correlation threshold was sufficiently low to include all of the features. Considerably more features were falsely mapped with the elevation values and the TPI compared with the hillshade and slope values. The diameter mapping accuracy for the synthetic DTM was improved, that is, more features were identified with correct diameters, and the deviations between the mapped diameters and the kiln-site diameters were lower for the variable combinations compared with the single variables. Relatively small, although numerous, deviations were produced by mapping using elevation. For the variable combinations, the best diameter mapping was achieved with combinations that included the slope.

An evaluation of the effects of specific object geometry disturbance types (Table 6) on the accuracy of diameter mapping suggests that the mapping quality was generally lowest for the incomplete kiln sites. For the kiln template without modelled disturbance and for the differences between the DTM and the template that included the added Gaussian noise to the model, the highest deviations were found for mapping using elevation. Using elevation further caused higher deviations for the irregular disturbances in the kiln-site surfaces and for sites with an adjacent spoil heap, whereas template matching using the hillshade exhibited a particularly high sensitivity to depressions in the kiln plateaus and partially filled ditches. Matching using the slope led to the highest deviations for the kiln plateau holes, which is depicted by the high slope values in the ideally planar kiln-relic surface. Moreover, the highest deviations for the kiln sites with completely filled ditches resulted when the TPI was used. When using variable combinations, the deviations were considerably smaller for the features with disturbed surfaces or disturbances in the ditches compared with the single variable results.

The mapping results for the synthetic DTM with Gaussian noise of different intensities (Figure 6) suggest that the noise affected the computed correlations to different extents depending on the variable used for mapping. Moreover, the object size affected the correlations. For elevation, the correlations clearly increased with the increasing feature diameter for all amounts of Gaussian noise. This relation was less clearly observed for the slope and the hillshade and was not observed for the TPI. The effect of moderate and high noise on the correlations was stronger for the slope, hillshade and TPI compared with the elevation (Figure 6a2 and a3) and indicates that the detection quality for these variables was more sensitive to noise in the DTM. The correlations were generally higher for the variable combinations (Figure 6b1–b3) than for the single variables, and were less dependent

Table 6. Sum of the deviations between mapped and feature diameters for the kiln templates (Ø =12 m, 18 m and 24 m) in a synthetic DEM; the table compares the results for single variables and variable combinations. The numbers in parentheses indicate the number of features that were not detected.

Variable	Undisturbed	Partially levelled on sloping terrain	Incomplete kiln site	Funnel hole	Irregular kiln plateau	Completely filled ditch	Partly filled ditch	Adjacent spoil heaps	Adjacent pits
Elevation	4	4	15	1	8	3	7	7	2
Hillshade	1	4 (2)	23 (1)	2 (2)	8	2 (1)	6	6	3 (1)
Slope	1	3	15	0 (3)	4	3	2	2 (1)	2 (2)
TPI	0	3 (2)	11 (1)	2	8	1 (1)	4	6	3
E–S	1	3	14	0	4	3	2	5	6
E–S–T	1	3	14	0	5	3	2	4	2
H–S–T	1	3	13	2	4	3	5	5	2
E–H–S–T	1	3	14	1	4	3	2	5	2

E, elevation; H, hillshade; S, slope; T, TPI.

DOI: 10.1002/arp

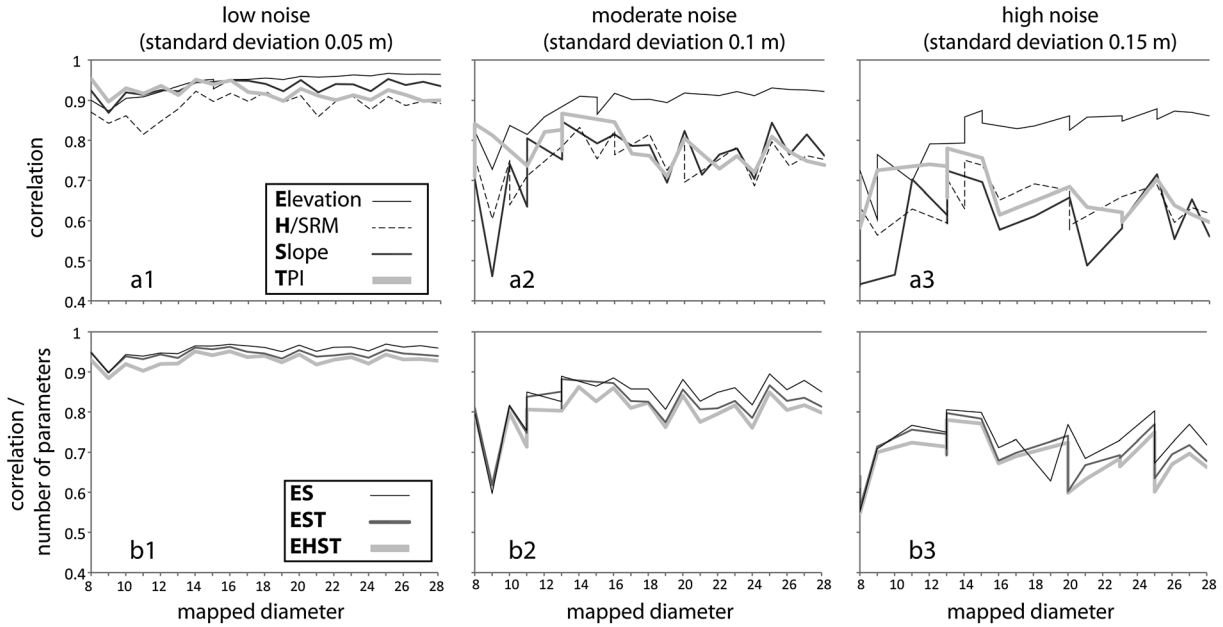

Figure 6. Correlation between the templates and the features in a synthetic DTM with Gaussian noise added at different intensities relative to the mapped diameter for the single variables (top) and the variable combinations (bottom). The *x* axes show the mapped feature diameters; missing or double correlation values for values of the *x* axis indicate false mapping of feature diameters.

on the feature diameter than those for the elevation values. All of the diameters were correctly mapped for low noise regardless of the variables used, whereas several diameters were falsely mapped for moderate and high noise (Figure 6). No considerable differences between the variables or the variable combinations were observed in this study.

Discussion

Suitability of the morphometric variables and variable combinations for feature detection

The evaluation results suggest that feature detection can be considerably improved, that is, the ratio of true to false detections can be increased using a combination of variables instead of the elevation or other morphometric variables alone. Regarding the number of true and false positive detections, the best performance was found for the *elevation–slope–TPI* combination.

By visually comparing the mapping results for each individual variable and variable combination with the kiln sites documented from the excavations and the hillshade maps, the characteristic limitations of successful detections for each variable can be further described. Typical examples for true and false detections using automated mapping with elevation values or the *elevation–slope–TPI* combination and using manual mapping in the Jänschwalde study area are shown in Figure 7. The features that were not detected using only elevation but were detected with the *elevation–slope–TPI* combination (Figure 7a1) primarily have an irregular topography, that is, the kiln relic was situated immediately adjacent to another kiln site, adjacent to pits or in linear depressions. False positive detections for the elevation data, which were not falsely detected using the *elevation–slope–TPI* variable combination (Figure 7a2), were primarily situated on the borders or crossings of paths and along linear structures resulting from forestry. In addition to the elevation values, the hillshade resulted in false detections for some of these features. A comparison of the results using automated mapping with the *elevation–slope–TPI* combination with those derived using manual mapping suggests that the automated mapping algorithm detected some additional kiln sites situated in irregular terrain, which is primarily due to the distraction of the human eye by these irregularities. The automated mapping method was not able to attain the manual mapping detection rates, especially for kiln relicts that were intersected by other morphologic structures, for example, those in linear depressions or those intersected by paths and tracks (Figure 7b1). Although many of these features were still detected using the hillshade or the TPI alone, considerably poorer results were achieved using the slope. Furthermore, many false detections on high and irregular heap

DOI: 10.1002/arp

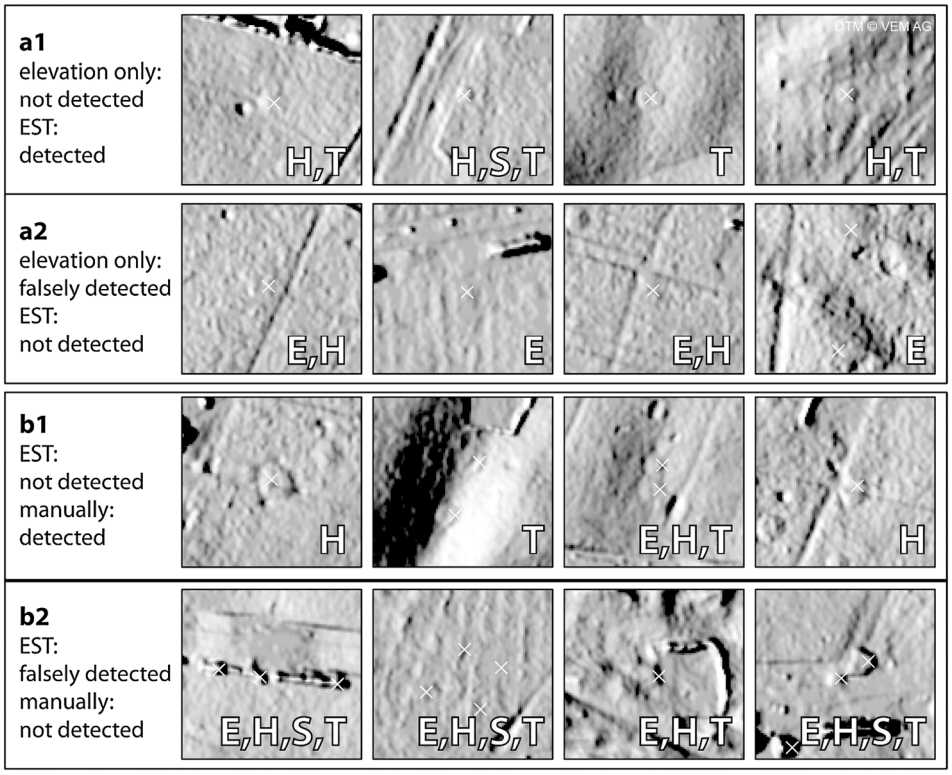

Figure 7. Characteristic kiln sites and other surface structures resulting in false negative and false positive detections for template matching using elevation and the combination elevation, slope and TPI (EST) compared with the manual mapping detections. The detections are shown on the Hillshade maps. The single variables for which the features were marked as detections are noted in the Hillshade map details (E, elevation; H, hillshade; S, slope; T, TPI).

structures and on planar areas in a sloping terrain that resulted from the automated detection could be distinguished easily from kiln sites by visual analysis and were not recorded by manual mapping (Figure 7b2). Most of these structures were also falsely mapped by at least three of the individual variables. A visual inspection of the mapping results further allowed characteristic false detections for the hillshade, slope and TPI to be determined. For all of the variables, high correlations and false detections resulted for spoil heaps and other mound structures. Characteristic false detections were observed on the western, that is, illuminated pit, sides using the hillshade, on planar areas in sloping terrain using the slope, and on track and path crossings using the TPI.

The mapping results from the ALS and the synthetic DTM and the computed correlations for the synthetic DTM (Table 4) confirm that deviations in the actual kiln-site geometry and the idealized feature geometry have different effects on the correlations depending on the variable used for template matching. For example, using the TPI for mapping resulted in a clearly lower sensitivity to variations in the slope of the terrain surrounding the kiln sites. This result can be explained by the template structure of the TPI, which accentuates the ditch and kiln plateau elevation relative to the surrounding terrain and does not represent large-scale variations in elevation (Figure 2b). The correlations for the slope were generally lower compared with those of the other variables, which can be explained by the fact that the slope map, which is the first derivative of the elevation map, enforces irregularities in the feature geometry. However, the correlations for the slope template exhibited relatively low sensitivity to variations in the structure of the ditch surrounding the kiln site (Table 4) because high slope values along the outer border of the kiln sites remain present despite these disturbances. In addition, the fact that the kiln-site diameters could be better approximated using the slope, hillshade or TPI compared with the elevation values may be due to the relatively substantial differences in these variables between the terrain surrounding the site and the outline of the kiln mound in contrast to gradual increases in elevation. Depending on the geometry of the mapped features, morphometric variables other than those evaluated in our study may improve template-matching techniques.

DOI: 10.1002/arp

Detection quality for the Jänschwalde test site

The ratio of false to true detections can be considerably improved in the study area using template matching with the *elevation–slope–TPI* variable combination compared with template matching using only elevation. In other studies, the reduction of false detections has been achieved primarily by post-processing the template-matching results. Trier and Pilø (2012) reduced false detections based on additional feature variables. Moreover, Nyström *et al*. (2014) applied linear discriminant analysis to reduce false detections. Similar to these approaches, elevation or slope thresholds within the mapped kiln-site polygons may be used to reduce false detections for the charcoal-kiln sites mapped in the Jänschwalde area, which is indicated by the differences in these variables observed for both true and false detections (Table 3). Without post-processing the matching results, Trier *et al*. (2009) suggested that detecting seven times as many false as true positives is a reasonable ratio for archaeological feature ring structures identified from aerial photographs. Based on template matching from high-resolution ALS data and post-processing using several additional feature variables, Trier and Pilø (2012) detected approximately 95% of a pit training dataset and approximately 3.8 times as many false than true positives using low correlation thresholds; approximately 86% of the features, along with slightly fewer false than true detections, were detected using medium correlation thresholds. Despite the lower elevation data resolution in our study, similar detection rates were obtained without post-processing the template matching results by mapping based on the *elevation–slope–TPI* variable combination (see Table 1). For kiln sites with diameters ≥9.5 m, approximately 98% of the manually mapped (i.e. detectable) sites were detected in addition to 3.7 times as many false than true detections at a correlation threshold of 0.4. Using a correlation threshold of 0.6 resulted in the detection of 74% of the detectable sites and fewer false than true detections. In studies focusing on the detection of trees by template matching (Pirotti, 2010; Nyström *et al*., 2014), the detection rates were much lower compared with those in our study or other studies that have focused on circular features. This difference may be due to the feature geometry and the necessity for template rotation when detecting non-circular features.

Relative to the diameters documented from the excavations, the kiln diameters were underestimated using both the manual and automated mapping techniques. However, this deviation can be partially explained by the characteristic kiln geometry (Figure 2a). In the excavations, the distance from the inner border of the ditch, which is mostly visible as a black circle in the sandy substrate of the study area, was recorded as the inner diameter. However, when mapping from the elevation models, the outermost border of the mound remaining from the kiln must be used to approximate this inner diameter. As the ditch around the kiln was not dug immediately adjacent to the kiln wood stack (cf. Figure 2a), a slightly smaller diameter of the remaining mound compared with the ditch's inner diameter is plausible. Our results show that the underestimation in the diameter was higher for automated mapping compared with manual mapping for small features, whereas a similar accuracy was achieved only with certain variable combinations for larger features (Table 2). Although the general detection results were improved using variable combinations for template matching compared with using single variables, combining variables did not generally result in a better feature diameter approximation. The results indicate that variable combinations based on the slope and TPI and not including the elevation values produced better mapping of feature sizes, which implies that variable combinations used for mapping can be adapted when mapping feature sizes is a central focus in a mapping campaign. The accuracy of mapped-feature sizes has been rarely discussed in other studies using template-matching approaches. Generally, it can be assumed that manual mapping from hillshade maps, especially over irregular terrain, can result in small displacements in the mapped features depending on the illumination angle. Therefore, an automated mapping approach based on variables that depict morphometric characteristics without position displacement and shadowing effects can be advantageous for an exact mapping of feature locations and boundaries.

Effects of the correlation threshold, terrain structure, feature size and DTM resolution

The mapping results for the Jänschwalde area prove that the ratio of true to false detections is highly dependent on the correlation threshold used in the mapping routine (Figure 5 and Table 1), which is in accordance with the results of Trier and Pilø (2012). The results of our study further indicate that a suitable correlation threshold must be specifically chosen depending on the variables used in the template-matching algorithm. Moreover, an evaluation of the correlation for mapped features with diameters of 8 m to 28 m in the DTM with added Gaussian noise (Figure 6) confirms that the correlation between the DTM and the elevation of the

DOI: 10.1002/arp

template increases with increasing feature diameter, that is, the effects of noise in the DTM are smaller for larger features. Although this relation was less clearly observable for the other variables, this result implies that the use of different correlation thresholds can be suitable depending on the template size when features for a wide range of sizes are mapped. Furthermore, the results for the synthetic DTM indicate that the correlations attained from the variable-combination template-matching approach are more affected by noise in the DTM, which may imply that feature detection can be most improved by variable-combination template matching with a low-noise DTM and that the variables used for template matching should be chosen depending on the DTM quality.

A comparison of mapping results for the area adjacent to the Jänschwalde mine with the hillshade map (Figure 8) suggests differences in the mapping quality for the different parts of the validation area; therefore, the limitations of automated mapping relative to the surface structure can be demonstrated for this area. The agreement between the automatically and manually mapped kiln sites and the excavated sites was high in the northern part of the area, corresponding to the area with relatively large kilns, a generally flat surface, few surface structures and little disturbance by earthworks (Figure 8a). The geomorphology of the southwestern region is characterized by linear drainage depressions that lead toward the Spree and Malxe River lowlands in the west (Figure 8b). In this area, lower detection rates were achieved by automated mapping compared with manual mapping. In the southern region, which is closest to the opencast mine, a considerably large number of structures from earthworks (spoil heaps and tracks) are represented in the elevation models. The presence of these structures resulted in many false detections produced by the automated routine, whereas the manual mapping technique produced relatively good results (Figure 8c). In the southeastern area, regular linear structures from forestry occur. Along with the small kiln-site diameters in this area, the detection rates using both the manual and automated mapping approaches were low (Figure 8d).

The detection quality for the manual and automated mapping approaches was highly dependent on the relation of the feature size to the DTM spatial resolution. For the 1 m DTM used in this study, the results show that circular objects with diameters of at least 9.5 m were mapped better than smaller features. Moreover, the detection quality further increased for features with diameters ≥11.5 m. We did not attempt to map objects smaller than 7.5 m in diameter because these features are represented by only a few DTM pixels and were not expected to be detectable. For the manual mapping of the same area, features with smaller diameters were identified (Raab *et al*., 2014); however, a validation against the excavation data also suggests a

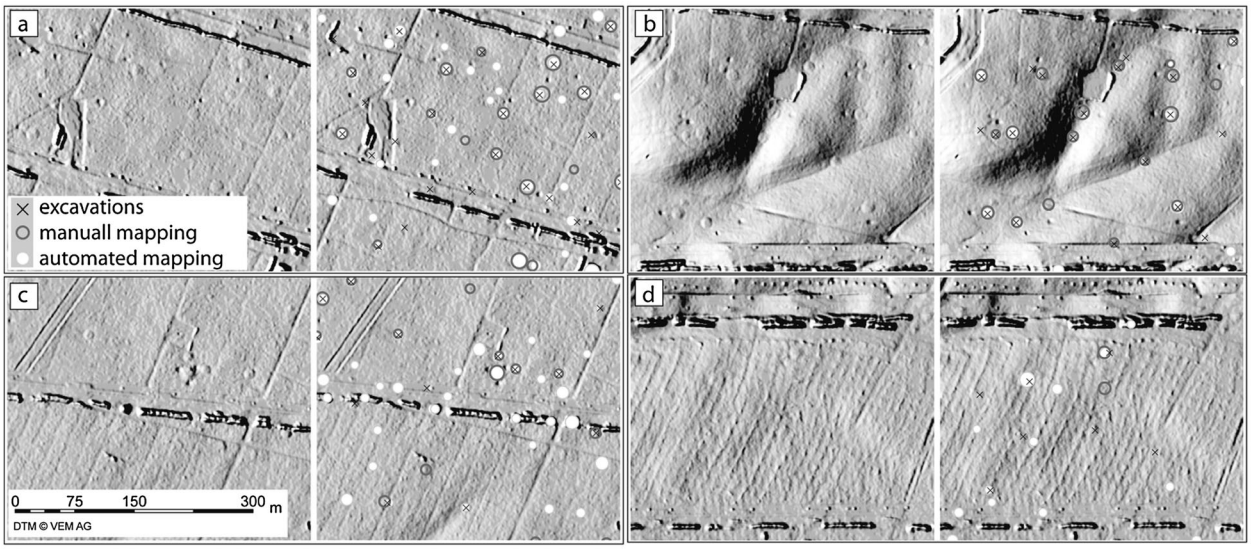

Figure 8. Kiln sites with diameters ≥9.5 m mapped using the automated routine (for the variable combination EST and a correlation threshold of 0.47), mapped manually and documented from excavations for different characteristic surface structures within the validation area: (a) for relatively flat and homogeneous terrain in which nearly all of the manually mapped kiln sites were automatically detected with a similar number of false detections; (b) for structured terrain with drainage lines that limited the detection by automated mapping; (c) for irregular terrain with structures from mine area earthworks and forestry, where considerably more false detections result from automated mapping; and (d) for irregular terrain with structures from forestry that limited the detection using both manual and automated mapping.

DOI: 10.1002/arp

relatively high uncertainty for these small structures. In a detailed evaluation of manual mapping from hillshade maps focusing on cultural remains of different size classes, Risbøl *et al*. (2013) found similar feature size effects for a 1 m DTM. Although a considerably low detection success rate was reported for features with diameters <7.5 m in this study, the results were slightly better for objects with diameters of 7.5–11.5 m and considerably better for features with diameters exceeding 11.5 m. For manual mapping of features with similar shapes and sizes as those examined in our study, Bollandsås *et al*. (2012) showed that more than three times as many true detections could be attained for different cultural remains by increasing the DTM resolution from one point to five points per square metre. For automated mapping with template matching, Trier and Pilø (2012) examined the relationship between the detection quality and the ALS datapoint density, and the results showed that the point-density reduction caused gradually decreasing detection rates as long as the point density exceeded 1.8 points per square metre. However, the authors also found that a rapid decrease in detection quality occurred for lower point densities.

Conclusions

In this study, a GIS-based automated routine for mapping small circular anthropogenic relief structures (i.e. charcoal kiln remains) was outlined. The routine is based on a template-matching approach and therefore can be applied to detect different symmetrical relief features with a characteristic geometry after constructing a suitable template. The mapping routine was evaluated for an ALS DTM of a field site in which excellent possibilities for validation were provided by large-scale archaeological excavations and previous studies that manually inspected hillshade maps. The effects of characteristic kiln-site irregularities and different degrees of DTM noise were further evaluated using synthetic elevation models. A DTM and DTM derivatives that distinguish kiln sites from the surrounding terrain, that is, hillshade, slope and TPI maps, were used for mapping. The automated mapping detections that were validated against the excavated and manually digitized kiln sites showed that template matching based on single variables resulted in considerable differences in the number of true and false detections for the elevation, slope, hillshade and TPI. The mapping results for the synthetic elevation models confirmed that the effects of feature geometry disturbances and DTM noise on the correlations between the idealized templates and the DTM vary for different morphometric variables. Based on these results, it was possible to identify an appropriate morphometric variable combination that improved the template-matching routine. The best results for the evaluation area were achieved using a combination of the elevation, TPI and slope. In particular, variable combination considerably reduced the number of false detections compared with mapping based on elevation values only, which clearly improves the practical applicability of the automated detection method for mapping high-density terrain features. Using the best variable combination, detection rates that were nearly identical to those attained using manual detection were achieved for kiln sites with diameters of at least 9.5 m in the validation area using elevation models with 1 m spatial resolution. Automated detection was less successful for smaller kiln sites, for which the number of false positive mapping results still considerably exceeded the number of true detections. A combination of the described automated routine and the removal of falsely detected sites using the DTM statistics or manual post-processing can considerably facilitate the mapping of small relief features from DTMs.

Acknowledgements

This study is a contribution to the Virtual Institute of Integrated Climate and Landscape Evolution Analysis (ICLEA) of the Helmholtz Association. This study was supported by the Brandenburg Ministry of Science, Research and Culture (MWFK) as part of the research group 'Anthropogenic Landscape Change and Palaeoenvironmental Research' and the International Graduate School of the BTU Cottbus-Senftenberg. The authors thank Vattenfall Europe Mining AG for providing the digital elevation models and the Brandenburgisches Landesamt für Denkmalpflege und Archäologisches Landesmuseum (BLDAM) for providing the archaeological data.

References

Bandeira L, Ding W, Stepinski TF. 2012. Detection of sub-kilometer craters in high resolution planetary images using shape and texture features. *Advances in Space Research* **49**(1): 64–74. DOI: 10.1016/j.asr.2011.08.021

Bennett R, Welham K, Hill Ra, Ford A. 2012. A comparison of visualization techniques for models created from airborne laser scanned data. *Archaeological Prospection* **19**(1): 41–48. DOI: 10.1002/arp.1414

Bollandsås OM, Risbøl O, Éne LT, Nesbakken A, Gobakken T, Næsset E. 2012. Using airborne small-footprint laser scanner data for detection of cultural

remains in forests: an experimental study of the effects of pulse density and DTM smoothing. *Journal of Archaeological Science* **39**(8): 2733–2743. DOI: 10.1016/j.jas.2012.04.026

Bond J. 2007. Medieval charcoal burning in England. In Arts and Crafts in Medieval Rural Environments, Klapste J, Sommer P (eds), 22–29 September 2005, *Ruralia* **VI**: Dobogókő, Hungary; 25–34.

De Laet V, Paulissen E, Waelkens M. 2007. Methods for the extraction of archaeological features from very high-resolution Ikonos-2 remote sensing imagery, Hisar (southwest Turkey). *Journal of Archaeological Science* **34**(5): 830–841. DOI: 10.1016/j.jas.2006.09.013

Deforce K, Boeren I, Adriaenssens S, Bastiaens J, De Keersmaeker L, Haneca K, Tys D, Vandekerkhove K. 2013. Selective woodland exploitation for charcoal production. A detailed analysis of charcoal kiln remains (ca. 1300–1900 AD) from Zoersel (northern Belgium). *Journal of Archaeological Science* **40**(1): 681–689. DOI: 10.1016/j.jas.2012.07.009

Devereux BJ, Amable GS, Crow P. 2008. Visualisation of LiDAR terrain models for archaeological feature detection. *Antiquity* **82**(316): 470–479.

Eisank C, Smith M, Hillier J. 2014. Assessment of multiresolution segmentation for delimiting drumlins in digital elevation models. *Geomorphology* **214**: 452–464. DOI: 10.1016/j.geomorph.2014.02.028

Groenewoudt B. 2005. Charcoal Burning and Landscape Dynamics in the Early Medieval Netherlands. *Ruralia* **IV**: 327–337.

Hesse R. 2010. LiDAR-derived local relief models – a new tool for archaeological prospection. *Archaeological Prospection* **17**(2): 67–72. DOI: 10.1002/arp.374

Jasiewicz J, Stepinski TF. 2013. Geomorphons – a pattern recognition approach to classification and mapping of landforms. *Geomorphology* **182**: 147–156. DOI: 10.1016/j.geomorph.2012.11.005

Jenness J, Brost B, Beier P. 2013. Land Facet Corridor Designer: Extension for ArcGIS. Jenness Enterprises. http://www.jennessent.com/arcgis/land_facets.htm date of access: 11.06.2014

Kennelly PJ. 2008. Terrain maps displaying hill-shading with curvature. *Geomorphology* **102**(3–4): 567–577. DOI: 10.1016/j.geomorph.2008.05.046

Lipsdorf J. 2001. Köhler über die Kohle. Ausgrabungen von Holzkohlemeilern am Tagebau Jänschwalde. *Ausgrabungen im Niederlausitzer Braunkohlenrevier - Arbeitsberichte zur Bodendenkmalpflege in Brandenburg* **8**: 213–223.

Ludemann T. 2003. Large-scale reconstruction of ancient forest vegetation by anthracology – a contribution from the Black Forest. *Phytocoenologia* **33**(4): 645–666

Menze BH, Ur JA, Sherratt AG. 2006. Detection of ancient settlement mounds: archaeological survey based on the SRTM terrain model. *Photogrammetric Engineering and Remote Sensing* **72**(3): 321–327.

Nelle O. 2003. Woodland history of the last 500 years revealed by anthracological studies of charcoal kiln sites in the Bavarian Forest, Germany. *Phytocoenologia* **33**(4): 667–682.

Nicolay A, Raab A, Raab T, Rösler H, Bönisch E, Murray AS. 2014. Evidence of (pre-)historic to modern landscape and land use history near Jänschwalde (Brandenburg, Germany). *Zeitschrift für Geomorphologie* **58**(Suppl. 2): 7–31. DOI: 10.1127/0372-8854/2014/S-00162

Nyström M, Holmgren J, Fransson JES, Olsson H. 2014. Detection of windthrown trees using airborne laser scanning. *International Journal of Applied Earth Observation and Geoinformation* **30**: 21–29. DOI: 10.1016/j.jag.2014.01.012

Open CV Development Team. 2014. OpenCV 2.4.9.0 Documentation. http://docs.opencv.org (accessed 27 May 2014).

Pirotti F. 2010. Assessing a template matching approach for tree height and position extraction from lidar-derived canopy height models of Pinus pinaster stands. *Forests* **1**(4): 194–208

Pollock R. 1998. Individual tree recognition based on a synthetic tree crown image model. In Proceedings of the International Forum on Automated Interpretation of High Spatial Resolution Digital Imagery for Forestry, Hill DA, Leckie DG (eds.). Victoria: British Columbia, Canada, February 10-12; 25–34.

Raab A, Takla M, Raab T, Nicolay A, Schneider A, Rösler H, Heußner K-U, Bönisch E. 2014. Pre-Industrial charcoal production in Lower Lusatia (Brandenburg, Germany) – detection and evaluation of a large charcoal burning field by combining archaeological studies, GIS-based analyses of shaded-relief maps and dendrochronological age determination. *Quaternary International*. DOI: 10.1016/j.quaint.2014.09.041

Risbøl O, Bollandsås OM, Nesbakken A, Ørka HO, Næsset E, Gobakken T. 2013. Interpreting cultural remains in airborne laser scanning generated digital terrain models: effects of size and shape on detection success rates. *Journal of Archaeological Science* **40**(12): 4688–4700. DOI: 10.1016/j.jas.2013.07.002

Rösler H. 2008. Köhlerei für das Eisenhüttenwerk Peitz in Brandenburg. *Archäologie in Deutschland* **3**: 36–37.

Rösler H, Bönisch E, Schopper F, Raab T, Raab A. 2012. Pre-industrial charcoal production in southern Brandenburg and its impact on the environment. In Landscape Archaeology between Art and Science, Kluiving S, Guttmann-Bond E (eds). Amsterdam University Press: Amsterdam; 167–178.

Salamunićcar G, Lončarić S, Pina P, Bandeira L, Saraiva J. 2014. Integrated method for crater detection from topography and optical images and the new PH9224GT catalogue of Phobos impact craters. *Advances in Space Research* **53**(12): 1798–1809. DOI: 10.1016/j.asr.2013.11.006

Sawabe Y, Matsunaga T, Rokugawa S. 2006. Automated detection and classification of lunar craters using multiple approaches. *Advances in Space Research* **37**(1): 21–27. DOI: 10.1016/j.asr.2005.08.022

Schindling J, Gibbes C. 2014. LiDAR as a tool for archaeological research: a case study. *Archaeological and Anthropological Sciences*. DOI: 10.1007/s12520-014-0178-3

Shruthi RBV, Kerle N, Jetten V. 2011. Object-based gully feature extraction using high spatial resolution imagery. *Geomorphology* **134**(3–4): 260–268. DOI: 10.1016/j.geomorph.2011.07.003

Sofia G, Fontana GD, Tarolli P. 2014. High-resolution topography and anthropogenic feature extraction:

testing geomorphometric parameters in floodplains. *Hydrological Processes* **28**(4): 2046–2061. DOI: 10.1002/hyp.9727

Stular B, Kokalj Z, Ostir K, Nuninger L. 2012. Visualization of lidar-derived relief models for detection of archaeological features. *Journal of Archaeological Science* **39**(11): 3354–3360. DOI: 10.1016/j.jas.2012.05.029

Tarolli P, Sofia G, Dalla Fontana G. 2012. Geomorphic features extraction from high-resolution topography: landslide crowns and bank erosion. *Natural Hazards* **61**(1): 65–83. DOI: 10.1007/s11069-010-9695-2

Trier ØD, Pilø LH. 2012. Automatic Detection of Pit Structures in Airborne Laser Scanning Data. *Archaeological Prospection* **19**(2): 103–121. DOI: 10.1002/arp.1421

Trier ØD, Larsen SØ, Solberg R. 2009. Automatic detection of circular structures in high-resolution satellite images of agricultural land. *Archaeological Prospection* **16**(1): 1–15. DOI: 10.1002/arp.339

Van Den Eeckhaut M, Kerle N, Poesen J, Hervás J. 2012. Object-oriented identification of forested landslides with derivatives of single pulse LiDAR data. *Geomorphology* **173–174**: 30–42. DOI: 10.1016/j.geomorph.2012.05.024

Verhagen P, Drăguţ L. 2012. Object-based landform delineation and classification from DEMs for archaeological predictive mapping. *Journal of Archaeological Science* **39**(3): 698–703. DOI: 10.1016/j.jas.2011.11.001